Aptamer conjugated Mo(6)S(9−x)I(x) nanowires for direct and highly sensitive electrochemical sensing of thrombin

ARTICLE *in* BIOSENSORS & BIOELECTRONICS · FEBRUARY 2010

Impact Factor: 6.41 · DOI: 10.1016/j.bios.2010.01.030 · Source: PubMed

Biosensors and Bioelectronics xxx (2010) xxx–xxx

Contents lists available at ScienceDirect

Biosensors and Bioelectronics

journal homepage: www.elsevier.com/locate/bios

Aptamer conjugated $Mo_6S_{9-x}I_x$ nanowires for direct and highly sensitive electrochemical sensing of thrombin

Martin McMullan[a], Nijuan Sun[b], Pagona Papakonstantinou[a,*], Meixian Li[b,**], Wuzong Zhou[c], Dragan Mihailovic[d]

[a] Nanotechnology and Integrated Bioengineering Centre, University of Ulster, Newtownabbey, Co. Antrim BT37 0QB, Northern Ireland, UK
[b] College of Chemistry and Molecular Engineering, Peking University, Beijing, 100871, PR China
[c] School of Chemistry, University of St Andrews, St Andrews KY16 9ST, Scotland, UK
[d] Jozef Stefan Institute, Jamova 39, SI-1000 Ljubljana, Slovenia

ARTICLE INFO

Article history:
Received 10 December 2009
Received in revised form 22 January 2010
Accepted 22 January 2010
Available online xxx

Keywords:
Aptamer sensors
MoSI nanowires
Self-assembly
Thrombin

ABSTRACT

We demonstrate the use of a novel electrochemical sensing platform based on aptamer conjugated $Mo_6S_{9-x}I_x$ nanowires (MoSI NWs) for the highly sensitive detection of the blood clotting enzyme thrombin. MoSI NWs nanowires were self-assembled on a gold electrode to which thrombin binding aptamers were covalently attached. The modification and immobilization steps of the electrodes were characterised by cyclic voltammetry along with high-resolution transmission electron microscopy and X-ray photoelectron spectroscopy. The platform is based on the creation of a self-assembled MoSI MW layer via the sulfur–gold affinity followed by the creation of MoSI-thiolated aptamer conjugates via the sulfur–sulfur affinity. Using this system, sensitive quantitative detection of thrombin is realized by monitoring differences of differential pulse voltammetric responses of electrostatically trapped $[Ru(NH_3)_6]^{3+}$ cations to the aptamer before and after thrombin binding. The sensitivity limit for the detection of thrombin is 10 pM. This value is 10-fold better than all currently reported one step label free electrochemical strategies. Given the direct label free nature of the approach and the simplicity of the electronic detection, the aptamer conjugated MoSI NWs biosensor appears well suited for implementation in portable point of care microdevices directed at the rapid and sensitive detection of proteins and pathogens.

1. Introduction

Combining sub-nanometer diameter with structural stability and interesting electronic properties, transition metal chalcogenide halide nanowires with stoichiometry $Mo_6S_{9-x}I_x$ (MoSI) and their analogues ($Mo_6S_{6-x}I_x$), have been discussed as a potentially viable alternative to carbon nanotubes for many applications (Kis et al., 2007; Ploscaru et al., 2007; Popov et al., 2008a; Strle et al., 2009; Vrbanic et al., 2004). MoSI NWs are fabricated in a single step process and form weakly bound bundles of parallel wires that exhibit metallic conductivity ($S_{300\,K} = 2 \times 10^3$ S/m) (Uplaznik et al., 2006). They can easily be dispersed in common solvents down to individual molecular wires. These properties make molybdenum sulfide NWs quite favorable building blocks for nanoscale electronic devices compared to carbon nanotubes (CNTs), for which a wealth of structural variants introduces widespread electronic properties, and the separation of single tubes from bundles is impeded by strong intertubular interactions (Nicolosi et al., 2007, 2005). Equally importantly, the sulfur terminators of MoSI nanowires act as "alligator clips" providing optimum contact to gold leads (Popov et al., 2008b) and thiolated proteins (Ploscaru et al., 2007) for molecular electronics applications. These properties also render MoSI nanowires useful for a variety of challenging investigations such as programmed materials assembly, the detection and quantification of trace analytes. Recently we showed that self-assembled nanocircuit architecture networks composed of sulfur–sulfur bridge connected MoSI NWs and thiolated anti-estrone antibodies provide an amplification and conductive pathway for the specific electrochemical sensing of estrone hapten (Sun et al., 2008).

In recent years, aptamers, single-stranded oligonucleotides, have been promoted as ideal diagnostic reagents and potential antibody replacements for the development of biorecognition nanosensors due to their high affinity, specificity and stability (Willner and Zayats, 2007). Currently, several aptamer-based analytical techniques for protein detection have been developed including chromatography (Zhao et al., 2008), colorimetry (Stojanovic and Landry, 2002), fluorescence (Bagalkot et al., 2007),

* Corresponding author. Tel.: +44 28 90368932; fax: +44 28 90366863.
** Corresponding author. Tel: +86 10 62757953; fax: +86 10 62751708.
E-mail addresses: p.papakonstantinou@ulster.ac.uk (P. Papakonstantinou), lmwx@pku.edu.cn (M. Li).

0956-5663/$ – see front matter. Crown Copyright © 2010 Published by Elsevier B.V. All rights reserved.
doi:10.1016/j.bios.2010.01.030

and surface enhanced Raman Spectroscopy, SERS (Cho et al., 2008). These existing assays, however, require slow, multistep processes and expensive instrumentation, which as a consequence limit their routine use. One interesting feature of many aptamers is that they undergo distinguishable conformational changes upon interactions with their ligands (Baker et al., 2006; Xiao et al., 2005b). Recently electrochemical aptamer-based sensors have exploited these binding induced conformational changes to monitor the interaction with ligands by measuring electron transfer to an interrogating electrode (Baker et al., 2006; Radi et al., 2006; Xiao et al., 2005a,b). A wide range of electrochemical/electronic aptamer-detection schemes have been described to date with the best achieving limits of detection ranging from picomolar to femtomolar (Bang et al., 2005; Hansen et al., 2006; He et al., 2007; Huang et al., 2008; Polsky et al., 2006; Zhou et al., 2007). While these detection limits are impressive, achieving them requires the integration of additional labels and often complicated sandwich configurations and amplification steps all of which make the detection complex, expensive and time consuming. There is an increasing interest in circumventing the labeling procedure and thereby providing a simple, rapid and low cost alternative (Sadik et al., 2009).

Here we describe an electrochemical sensing platform for the highly sensitive, label free detection of thrombin, a critical protease in the blood coagulation cascade. The platform is based on the creation of a self-assembled MoSI MW network via the sulfur–gold bond affinity followed by the creation of MoSI-thiolated aptamer conjugates via the sulfur–sulfur affinity. Using this system, sensitive quantitative detection of thrombin is realized by monitoring differences of differential pulse voltammetric responses of electrostatically trapped $[Ru(NH_3)_6]^{3+}$ cations to the negatively charged phosphate backbone of the conjugated aptamer before and after thrombin binding. The binding of the positively charged thrombin with the aptamer reduced the surface concentration of the electrostatically bound cationic ions ($[Ru(NH_3)_6]^{3+}$) and decreased their voltammetric response. As a result our described aptamer-based sensor allows a much simpler detection scheme, coupled with a lower detection limit, when compared to other techniques based on multiple binding events and complex labeling.

2. Experimental

2.1. Chemicals and materials

The thrombin binding aptamer (TBA) with an active end thiol group and the five additional nucleotides (T5) spacer was modified to the 5′-end of the 15-mer DNA aptamer (5′-SH-CCAAC GGT TGG TGT GGT TGG). It was obtained from TIB Molbiol (Germany) and reconstituted with Tris-EDTA pH 7.4, 10 mM (Fluka, UK). Subsequent dilutions were prepared using phosphate buffer saline (PBS) solution (0.5 M, pH 7.4). Human-thrombin (p$I \approx 7.3$) 1710 NIH unit/mg, MW 37423) and hexammineruthenium (III) chloride [$Ru(NH_3)_6Cl_3$, 98+%] were purchased from Sigma and Aldrich respectively. Trizma hydrochloride and NaCl were obtained from Sigma. Aqueous solutions were prepared with autoclaved Millipore Milli-Q water (15 MΩ cm). Gold electrodes were from Nanobio, Singapore.The synthesis of $Mo_6S_{9-x}I_x$ nanowires (Vrbanic et al., 2004) was performed in a sealed and evacuated quartz ampoule, from platelets of Mo sheet metal (e.g. Aldrich, molybdenum foil 0.1 mm thick, 99.9+%), sulfur powder (99.98%) and I_2 (Aldrich, 99.999%) in the desired stoichiometric amounts. The ampoule was heated to a temperature of 1070 °C at a rate of 8 K/h and kept at this temperature for 72 h. The ampoule was then cooled at 1.5 K per min. The resulting material had a fur-like appearance, where the diameter of individual bundles ranged from 100 nm to 1000 nm and their lengths up to 5 mm. In this work all studies were carried out on $Mo_6S_3I_6$ nanowires. Redox probe solution of $[Ru(NH_3)_6]^{3+}$ was prepared by dissolving it in trizma hydrochloride (10 mM, pH 7.4) solution, and 50 mM NaCl added as the supporting electrolyte.

2.2. Fabrication of MoSI nanowire aptasensor

MoSI dispersions of 1 mg ml^{-1} in isopropanol were initially sonicated for 2 min using a high power ultrasonic tip (120 W, 60 kHz) followed by a mild sonication for 2 h using a low power ultrasonic bath. Prior to use, the dispersions were re-sonicated for 20 min to obtain uniform suspension, which was denoted as MoSI NWs suspension.

Gold electrodes (AuE) were successively polished with a microcloth coated with suspensions of alumina slurries (Buehler) of 1 μm, 0.3 μm and 0.05 μm respectively. The polished electrodes were then sonicated for 5 min in deionised water to remove any remaining polishing agent. A smooth gold surface is important to support efficient NW binding (Willner and Zayats, 2007). Electrodes were then scanned under basic conditions (0.5 M NaOH) with a scan rate of 2 V s^{-1} over the potential range −0.35 to −1.35 V to clean the electrodes before sensor fabrication. The cleaning process is completed when the scans become constant and no further changes in peak height or shape are observed (typically 500 scans). Then oxidation and reduction scans under acidic conditions (0.5 M H_2SO_4) over the potential range −0.1 to 1.7 V (60 scans at a scan rate of 0.5 V s^{-1}) were conducted. Finally the electrode was placed in 1 mg ml^{-1} MoSI NW suspension for 12 h to form a self-assembled NW layer on the gold surface, then washed with isopropanol and dried. This modified electrode is denoted as NW/AuE. Aptamer conjugated electrodes were prepared by placing the NW/AuE into 100 nM thiolated aptamer solution for 12 h under ambient conditions. Electrodes were then washed with PBS (0.5 M, pH 7.4) and water and dried under N_2 before characterization.

2.3. Optimization of aptasensor conditions

In order to achieve optimal sensor performance, several factors that influence the affinity binding between the immobilized aptamer and thrombin and their electrostatic interactions with redox cations must be considered.

Other important factors include incubation time, temperature and concentration of aptamer binding target protein. The concentration of TBA used to modify the AuE/NW was in the range of 10–500 nM. It was observed that the peak currents of DPV measurements were saturated at concentrations above 100 nM. The effect of temperature on the aptasensor binding with a fixed concentration of thrombin (100 nM) was investigated. The current responses increased as the temperature was raised from 20 °C to 35 °C, followed by a fall upon further temperature increase. With the increased incubation time, the response of the aptasensor to thrombin also increased, reaching a plateau at about 30 min. Longer incubation time did not improve the response.

2.4. Instrumentation

The electrochemical measurements were performed by using an Autolab PGSTAT 10 potentiostat/galvanostat (Eco Chemie, Netherlands) driven by GPES*v* 4.9 software package and connected to an electrochemical cell in a standard three electrode arrangement. The working electrode was a gold electrode with a diameter of 1 mm. A 3 M NaCl Ag/AgCl electrode was used as the reference electrode and a Pt wire as the counter electrode, respectively. Measurements were performed in 50 mM NaCl/10 mM Tris buffer solution, pH 7.4, in the presence of 2 μM $[Ru(NH_3)_6]^{3+}$ as redox probe, at room temperature. The cyclic voltammetric (CV) measurements were performed at a scan rate of 100 mV s^{-1} in the potential range

Please cite this article in press as: McMullan, M., et al., Biosens. Bioelectron. (2010), doi:10.1016/j.bios.2010.01.030

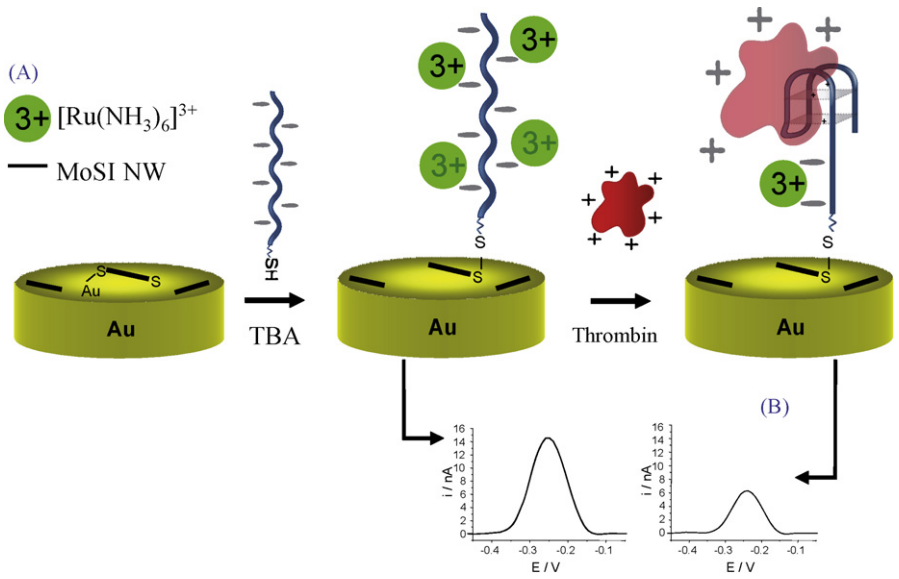

Scheme 1. (A) Schematic diagram of the detection method and preparation steps of the aptasensor (a) nanowires are self-assembled on a Au electrode through gold–thiol bonds by incubating the Au electrode in a MoSI NW dispersion followed by a rinsing step removing physisorbed NWs; (b) NW/Au electrode immobilised with 100 nM TBA. A thiol-modified single stranded TBA attached to NW is naturally unfolded in the absence of human a thrombin target molecule. The unfolded TBA is chemisorbed on the NW surface through S–S bonds. A low concentration of $[Ru(NH_3)_6]^{3+}$ cations allows the detection of surface-controlled waves; (c) thrombin is incubated on the prepared TBA-NW/Au platform followed by a rinsing step removing physisorbed TBA. In the presence of thrombin, TBA changes conformation into a G-quadruplex form resulting in a prompt decrease of adsorbed cations, and hence a decrease of the detection signal. (B) Electrochemical performance of electrode monitored by DPV for thrombin quantification.

of 0.2 to −0.6 V, with the differential pulse voltammetric (DPV) measurements carried out in the same potential range at a scan rate of 10 mV s^{-1}. After each experiment the electrode was rinsed with Tris buffer and small amounts of water. A Savitzky and Golay smoothing technique was employed for the DPV results along with baseline correction with a moving average peak width of 0.01 V. The electrolyte solution was degassed with N_2 for 5 min, with all experiments conducted under nitrogen atmosphere.

High-resolution transmission electron microscopy (HRTEM) characterizations were performed using a JEOL 2010 operating at 200 kV accelerating voltage (with a point resolution of 2 Å). Samples were prepared by dropping MoSI NW suspensions onto 300 mesh copper, holey carbon film (Agar), allowed to dry and rinsed with IPA. Aptamer modified NW sample was prepared as above, with the TEM grid immersed in 100 nM aptamer for 12 h and washed with water.

X-ray photoelectron spectroscopy (XPS) was performed with a Kratos (Manchester, UK) Axis Ultra DLD spectrometer. A monochromated Al anode (150 W) was used as the X-ray source. The S 2p spectra were recorded from cleaned 5 mm × 5 mm silicon substrates with 80 μl of MoSI NW dispersions drop dried under an IR lamp. The modified sample was placed in 100 nM aptamer for 12 h and subsequently was washed with water and dried under nitrogen.

3. Results and discussion

3.1. Construction and characterization of the aptasensor

Scheme 1 illustrates the construction of the NW aptasensor. This involves (i) formation of MoSI NW self-assembled layer on the gold surface through the gold–sulfur covalent chemistry bonding, (ii) covalent association of the thiolated thrombin binding aptamer to NWs through the sulfur–sulfur bonding and (iii) capture of thrombin through incubation of modified electrode in varying concentrations of thrombin.

The MoSI-TBA assembly was characterised by HRTEM. Sonicated dispersions of 1 mg ml^{-1} NWs in isopropanol formed multiple-strand bundles with average diameters of 50–200 nm on TEM grids. Fig. 1a shows typical morphology of the bare MoSI NWs. The surface of the NWs is relatively clean without significant deposition of an amorphous coating. Fig. 1b is a HRTEM image of the bare MoSI nanowires. The measured *d*-spacings and the interplane angle indicate that the *d*-spacings can be indexed into a hexagonal unit cell with cell parameters $a = 1.83$ and $c = 1.05$ nm. The crystal structure is similar to that of $Mo_6S_{9-x}I_x$ in previous reports (Vrbanic et al., 2004) and is a double-fold superstructure based on a unit cell reported by (Nicolosi et al., 2007). In Fig. 1c and d, the NW sample exposed to 100 nM TBA, has a significantly different appearance, where the presence of nodule like projections (diameters 5–10 nm) along NW is evident. This result indicates that immobilization is not limited at the ends of the nanowires but is also possible throughout the whole surface of the nanowire. Chemisorbed TBA bound through a covalent sulfur–sulfur bond, remains immobilized on the nanowire surface after rinsing with PBS for several times.

The covalent attachment of the thiolated TBA to MoSI NW through the S–S bonding was confirmed by comparison of MoSI NWs XPS spectra in the presence and absence of TBA. The S 2p XPS signal of NWs was deconvoluted into four components located at 161.5, 163.1, 164.5 and 169.1 eV respectively as shown in Fig. 2a. The peaks at 161.5 and 163.1 eV, which correspond to sulfur $2p_{5/2}$ and $2p_{3/2}$ spin–orbit splitting, are indicative of metal sulfide and can be attributed to MoS_x. The broad peak at 169.1 eV is associated with oxygenated sulfur moieties (SO_2, S_2O_3, SO_3, SO_4, etc.) (Colvin et al., 1992). The first two peaks ($S2p_{5/2}$ $S2p_{3/2}$) decreased in magnitude possibly due to the blocking effect of TBA, whereas the last one increased significantly in the NW/TBA sample as illustrated in Fig. 2b. The S $2p_{1/2}$ component at approximately 164 eV corresponds to a disulfide bond (Castner et al., 1996; Wang and Lieberman, 2003). The increase of this component with respect to $S2p_{5/2}$, $S2p_{3/2}$ peaks upon the association of TBA to MoSI NWs, is attributed to the formation of S–S bonding between the MoSI NW and the aptamer.

Please cite this article in press as: McMullan, M., et al., Biosens. Bioelectron. (2010), doi:10.1016/j.bios.2010.01.030

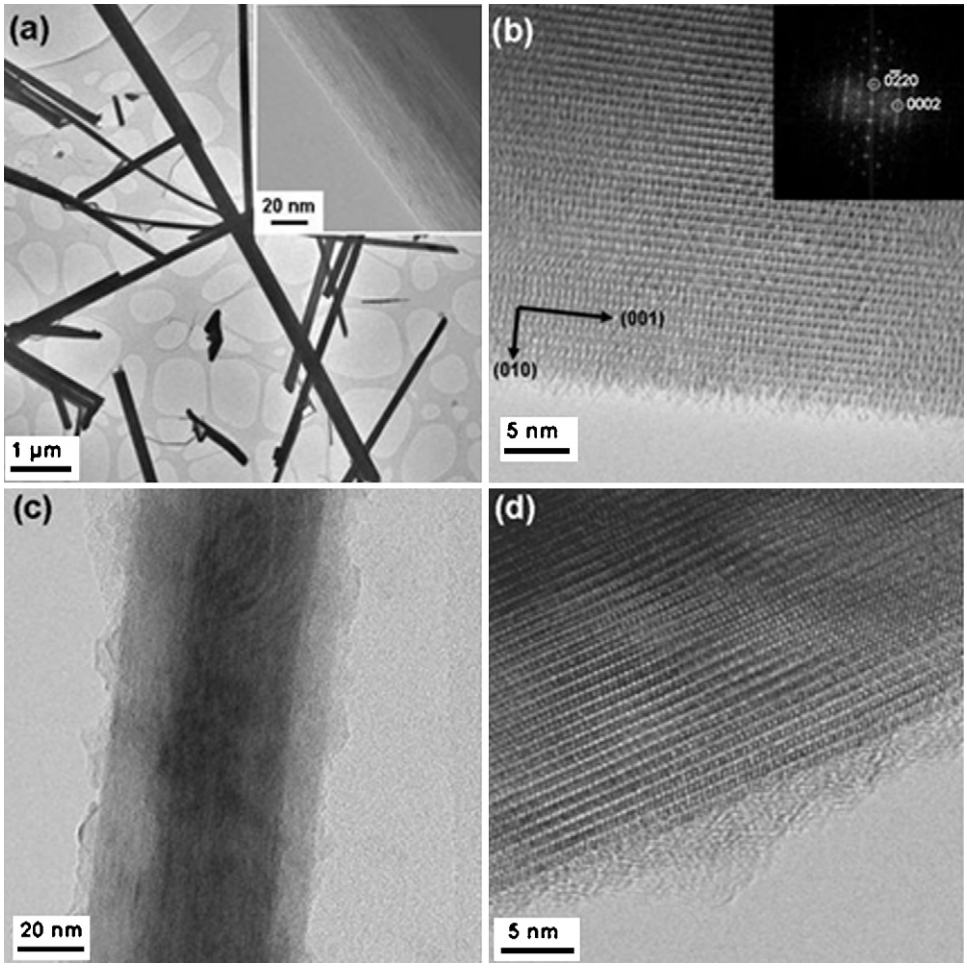

Fig. 1. (a) TEM image of bare MoSI NWs dispersed on a holey carbon film. The inset is an enlarged TEM image showing a surface of NW. (b) HRTEM image viewing down the [10–10] zone axis. The inset is the corresponding FFT diffraction pattern indexed to a hexagonal unit cell with $a \approx 1.83$ nm and $c \approx 1.05$ nm. (c and d) HRTEM images of MoSI NW after immobilization with 100 nM thiolated TBA.

3.2. Detection principle

The detection principle of the sensor is based on translating the conformational change of the aptamer upon target binding, directly into a measurable signal through the use of cationic redox active reporting units that are bound electrostatically with the DNA aptamer phosphate backbone. First, thiolated anti-thrombin aptamers are conjugated onto the NW/AuE via self-assembly. In the absence of thrombin, the interaction between redox reporters and conjugated unfolded aptamers yields a prominent voltammetric response. Upon binding with thrombin, the aptamer is folded into its inherent tertiary structure namely G-quadruplex—resulting in a reduced signal since the $[Ru(NH_3)_6]^{3+}$ ions can only bind to the DNA aptamer phosphate backbone where thrombin does not occupy. Thus the binding of positively charged thrombin with the aptamer reduces the overall density of negative charges, leading to a decrease in the density of cationic reporting units and a corresponding decline in the electrochemical response.

In our approach, the detection of thrombin is realized by exploiting the prospensity of $[Ru(NH_3)_6]^{3+}$ ions to electrostatically bind to the negatively charged aptamer surface and subsequent determination of their surface-confined electrochemical response. It is well known that for surface-confined redox species, the anodic-to-cathodic peak current ratio in a cyclic voltamogram is close to unity, and a linear relationship between the scan rate and the current intensity is expected. This diagnostic procedure will ensure that the species detected on the electrode surface correspond to those confined on the surface of the electrode and not those present in the bulk of the solution (diffusion controlled). If a linear relationship between the square root of scan rate and the current intensity is found this would indicate that the electrode reaction is controlled by diffusion, which is the mass transport rate of the redox species to the surface of the electrode across a concentration gradient. A key attribute of this sensor is the selection of appropriate micromolar concentrations of $[Ru(NH_3)_6]^{3+}$ molecules at which the distinction of surface-controlled waves from diffusion-controlled waves is possible (Cheng et al., 2007). The redox concentration should not be too high as this would result in the detection of diffusion-controlled waves of $[Ru(NH_3)_6]^{3+}$. In a low ionic strength solution of $[Ru(NH_3)_6]^{3+}$ the cations produce an ion exchange equilibrium between the probe and the native charge compensation ions (Na^+) associated with the anionic DNA backbone (Yu et al., 2003). For this study, concentrations in the range of 2–50 μM were tested, where CV scans indicated 2 μM $[Ru(NH_3)_6]^{3+}$ was suitable for ensuring significant surface-controlled waves without appearance of diffusion-controlled waves for the redox probe. Confirmation of the surface-confined species was determined from scan rate dependence studies. Fig. S1 shows plots of anodic peak current as a function of scan rate (ν), where a linear response is observed for 2 μM $[Ru(NH_3)_6]^{3+}$ (Fig. S1a), demonstrating a surface-controlled electrode process. This is in contrast to a $\nu^{1/2}$ linear dependence which is representative of Nernst waves of diffusing species (Bard and Faulkner, 2001). The non-linear response at the higher concentration of 50 μM $[Ru(NH_3)_6]^{3+}$ shown in Fig. S1b, is indicative of a

mass-transfer limited reaction (Bard and Faulkner, 2001; Steel et al., 1999).

3.3. Performance of the aptasensor

Each step of the fabrication process of the aptasensor was characterised by cyclic voltammetry using 2 μM of $[Ru(NH_3)_6]^{3+}$ as redox probe (Fig. 3A). Voltammograms were generally stable after the fourth cycle, where a gradual increase of the cathodic and anodic peak currents was observed, indicating progressive adsorptive accumulation at the surface (Bard and Faulkner, 2001). At the bare AuE, both anodic and cathodic peaks are weakly defined at this concentration, similar to the reported literature (Cheng et al., 2007), with a peak separation (ΔE_p) of 111 mV, as shown in Fig. 3A, curve (a), however, upon self-assembly of the MoSI NWs on the gold surface, the peak separations were reduced to (ΔE_p) 41 mV (Fig. 3A, curve (b)). Following the attachment of TBA, a further reduction was observed, forming negligible peak separations (Fig. 3A, curve (c)). This behaviour is indicative of a surface-controlled process, as the separation between the peak potentials is smaller than that expected for solution-phase processes. Ideal Nernstian behaviour of surface-confined non-reacting species is demonstrated by symmetric CV peaks ($\Delta E_p = 0$) (Bard and Faulkner, 2001). A reduced peak separation was also obtained for the TBA/AuE electrode (no MoSI NW), shown in Fig. 3B, curve (b), however it does display greater separation ($\Delta E_p = 40$ mV) than the MoSI NW modified electrode. This peak-to-peak separation may be attributed to the slower kinetics of charge transfer of bare Au electrode (Radi et al., 2006), when compared to the MoSI NWs modified electrode.

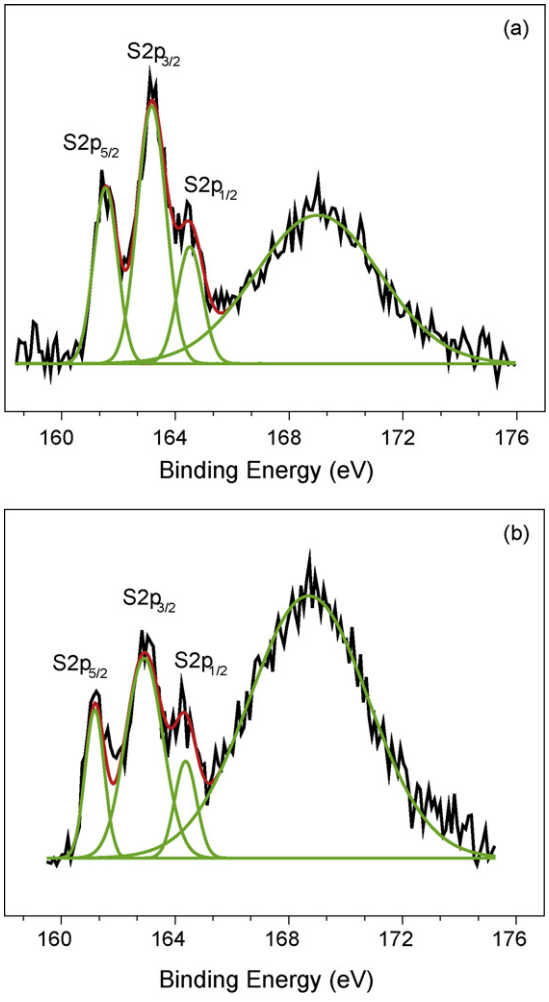

Fig. 2. X-ray photoelectron spectra of the S_{2p} region of MoSI NWs on silicon substrates (a) bare MoSI NW and (b) MoSI NW immobilised with 100 nM TBA. The peaks were fitted by functions describing doublets with spin–orbit coupling components, using Gaussian fitting and a linear background.

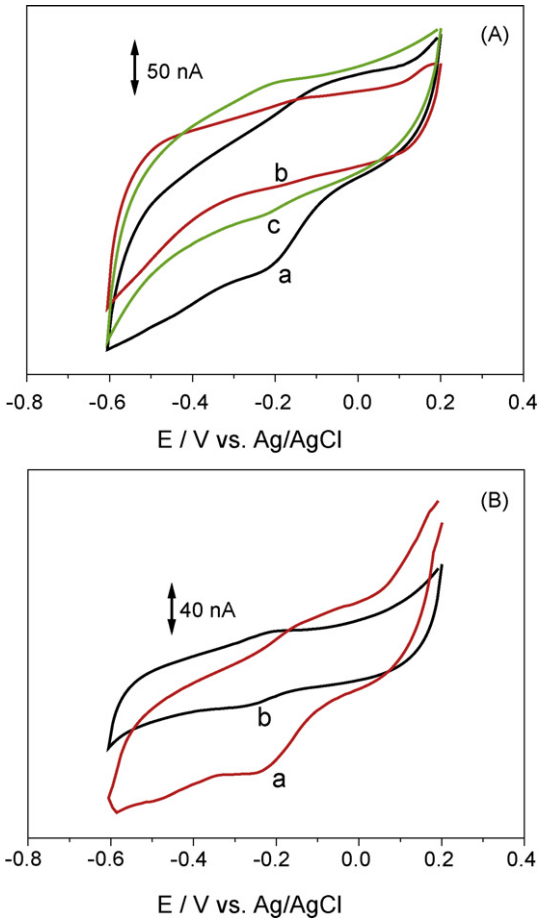

Fig. 3. Cyclic voltammograms of 2 μM $[Ru(NH_3)_6]^{3+}$ redox probe characterizing modification steps of the Au electrode at a scan rate of 100 mV s^{-1}. (A) A bare Au electrode (a) modified with MoSI NWs (b) and incubated with 100 nM TBA (c); (B) the bare Au electrode (a) modified with 100 nM TBA only (b).

Thrombin was chosen as a target protein to demonstrate our strategy. Incubation of the electrode with thrombin resulted in a decrease of the redox peaks and in particular, in the oxidation peak current which can be taken as a quantitative measure of protein concentration. This behaviour was investigated by DPV, providing much higher sensitivity than conventional sweep techniques. The higher sensitivity in DPV is due to the fact that the measured current is only a product of the faradaic process, with the capacitive charging current eliminated greatly (Bard and Faulkner, 2001; Radi et al., 2006).

Fig. 4 shows the DPV responses of the TBA/NW/Au modified electrode when incubated with thrombin. This interaction with thrombin causes significant conformational changes to the TBA, folding into its secondary, chair-like quadruplex/duplex while keeping the target molecules stabilized by intermolecular hydrogen bonds (Li et al., 2007). As a result there are changes in the charged surface of the aptamer. Association of thrombin with the aptamer blocked the adsorption of the redox probe $[Ru(NH_3)_6]^{3+}$ and depleted its voltammetric response. Based on this principle, the performance of the aptasensor was evaluated by incubation of the electrode in varying thrombin concentrations of 1 fM to 100 nM. Increasing concentrations of thrombin resulted in a decreased cur-

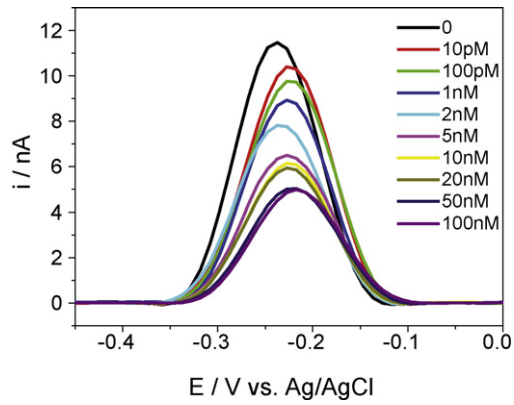

Fig. 4. Differential pulse voltammograms of the TBA/NW/Au modified electrode incubated in different concentrations (from 10 pM to 100 nM) of thrombin. Scan rate is 10 mV s^{-1}.

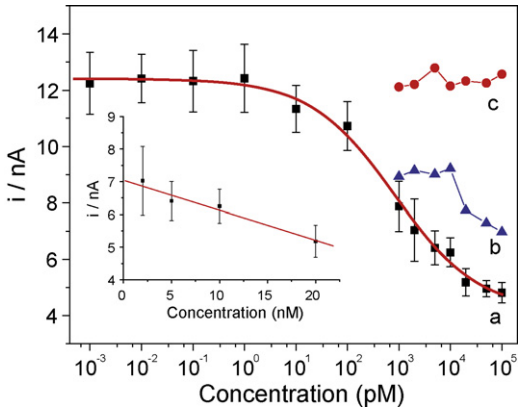

Fig. 5. Calibration curves for the current responses of different concentrations of thrombin on the TBA/NW/AuE (a), TBA/AuE (b) and calibration curve for the current responses of different concentrations of BSA on the TBA/NW/AuE (c). The inset shows the linear part of curve (a).

rent response of the modified electrode.

The sigmoid curve presented in Fig. 5, shows the peak current versus thrombin concentration in logarithmic scale, where each point corresponds to the average of three independent measurements. The aptasensor shows a linear response range from 2.0 nM to 20 nM with a correlation coefficient of $r = 0.981$. When thrombin concentration was increased to 50 nM and above, the signal began to level off, suggesting most of the TBA probes have been associated with the thrombin target. This particular range allows for thrombin analysis within clinically relevant concentrations where the serine protease is produced in nanomolar concentrations (Li et al., 2007). The detection limit was measured as 10 pM (0.37 ng ml^{-1}), comparing favorably with other studies (Bini et al., 2007; Li et al., 2008; Liss et al., 2002; Sánchez et al., 2006; Willner and Zayats, 2007). The relative standard deviation for the target concentrations of 10 nM was 7% by five replicate measurements, indicating that the sensor is quite reproducible.

3.4. Selectivity

In order to determine the influence and role of MoSI NWs on the specific interaction between TBA and thrombin, a control experiment was designed involving all the steps in the construction process except the use of MoSI NW. With this arrangement the protocol was also capable of detecting thrombin, however, the detection limit for this TBA/AuE was 20 nM as shown in curve (b) of Fig. 5, which is three orders of magnitudes higher than the detection limit of the TBA/NW/AuE. Furthermore, to verify that the signal change is dependent on the specific recognition of thrombin, we added a nonspecific bonding protein, bovin serum albumin (BSA). The resulting current changes for different concentrations of BSA were irregular and insignificant, as shown in curve (c) of Fig. 5. This suggests that no conformational change was induced as TBA did not bind to BSA confirming that the quantification of thrombin is a consequence of a specific interaction. Taken together, these observations indicate that the presence of MoSI NWs provide significant amplification of the highly specific detection of TBA–thrombin interaction. Crucially, for use as molecular connectors, MoSI NWs have S atoms at their surfaces, allowing covalent bonds to be formed with both gold and thiolated aptamer. This together with their high surface to volume ratio and metallic behaviour make them highly sensitive to minor surface perturbations, forming an easily and effectively modified sensor.

4. Conclusions

In summary, we have demonstrated a novel electrochemical sensor based on aptamer conjugated $Mo_6S_{9-x}I_x$ nanowires (MoSI NWs) self-assembled on a gold electrode for the direct, highly sensitive and specific detection of the coagulation protein thrombin. Our approach is less sensitive than some established methods for detecting thrombin, such as chromatography or colorimetric enzymatic assays. These existing assays, however, require slow, multistep processes and expensive instrumentation, and thus our approach appears much more convenient. The sensing mechanism is based on a single step thrombin binding event to aptamer, which results in a decrease of the intensity of the voltammetric signal of the redox probe molecule ($[Ru(NH_3)_6]^{3+}$), attached electrostatically to the DNA phosphate backbone of the aptamer. The proposed sensor provides linear response between 2.0 nM and 20 nM with a detection limit of 10 pM. This value is 10-fold better than all currently reported one step label free electrochemical strategies. The high sensitivity of the MoSI NWs aptamer-based sensor is related to the following unique attributes: (a) the MoSI NWs provide a high density of sulfur sites and hence a high density of thrombin binding aptamers (Fig. S2) (b) Moreover, the immobilization of thrombin binding aptamer on the NW surfaces is achieved through covalent binding (via the sulfur–sulfur bond), rather than simple adsorption, which always gives rise to instability like problems (c) the highly conductive MoSI NWs provide a direct electrical path way for the electrochemical sensing of thrombin. The method can be easily extended to other aptamers with specific conformational change during the recognition between the aptamer and its target. Given the simplicity and direct label free nature of the approach, it is expected that this aptamer conjugated MoSI NW biosensor will be widely applicable to the development of rapid, aptamer-based electronic sensors for a number of analytes of biomedical and/or environmental importance.

Acknowledgements

This work has been supported by Royal Society (UK–China Joint Project, JP052544), the National Natural Science Foundation of China (20875005 and 20735001), the EPSRC through the free access to Materials Research equipment services and the GlaxoSmithKline, which provided a CAST PhD studentship to Martin McMullan.

Appendix A. Supplementary data

Supplementary data associated with this article can be found, in the online version, at doi:10.1016/j.bios.2010.01.030.

References

Bagalkot, V., Zhang, L., Levy-Nissenbaum, E., Jon, S., Kantoff, P.W., Langer, R., Farokhzad, O.C., 2007. Nano Lett. 7 (10), 3065–3070.
Baker, B.R., Lai, R.Y., Wood, M.S., Doctor, E.H., Heeger, A.J., Plaxco, K.W., 2006. J. Am. Chem. Soc. 128 (10), 3138–3139.
Bang, G.S., Cho, S., Kim, B.-G., 2005. Biosens. Bioelectron. 21 (6), 863–870.
Bard, A.J., Faulkner, L.R., 2001. Electrochemical Methods, second ed. Wiley.
Bini, A., Minunni, M., Tombelli, S., Centi, S., Mascini, M., 2007. Anal. Chem. 79 (7), 3016–3019.
Castner, D.G., Hinds, K., Grainger, D.W., 1996. Langmuir 12 (21), 5083–5086.
Cheng, A.K.H., Ge, B., Yu, H.Z., 2007. Anal. Chem. 79 (14), 5158–5164.
Cho, H., Baker, B.R., Wachsmann-Hogiu, S., Pagba, C.V., Laurence, T.A., Lane, S.M., Lee, L.P., Tok, J.B.H., 2008. Nano Lett. 8 (12), 4386–4390.
Colvin, V.L., Goldstein, A.N., Alivisatos, A.P., 1992. J. Am. Chem. Soc. 114 (13), 5221–5230.
Hansen, J.A., Wang, J., Kawde, A.N., Xiang, Y., Gothelf, K.V., Collins, G., 2006. J. Am. Chem. Soc. 128 (7), 2228–2229.
He, P., Shen, L., Cao, Y., Li, D., 2007. Anal. Chem. 79 (21), 8024–8029.
Huang, Y.C., Ge, B., Sen, D., Yu, H.-Z., 2008. J. Am. Chem. Soc. 130 (25), 8023–8029.
Kis, A., Csanyi, G., Vrbanic, D., Mrzel, A., Mihailovic, D., Kulik, A., Forró, L., 2007. Small 3 (9), 1544–1548.
Li, T., Li, B., Dong, S., 2007. Chem. Eur. J. 13 (23), 6718–6723.
Li, X., Shen, L., Zhang, D., Qi, H., Gao, Q., Ma, F., Zhang, C., 2008. Biosens. Bioelectron. 23 (11), 1624–1630.
Liss, M., Petersen, B., Wolf, H., Prohaska, E., 2002. Anal. Chem. 74 (17), 4488–4495.
Nicolosi, V., Nellist, P.D., Sanvito, S., Cosgriff, E.C., Krishnamurthy, S., Blau, W.J., Green, M.L.H., Vengust, D., Dvorsek, D., Mihailovic, D., Compagnini, G., Sloan, J., Stolojan, V., Carey, J.D., Pennycook, S.J., Coleman, J.N., 2007. Adv. Mater. 19 (4), 543–547.
Nicolosi, V., Vrbanic, D., Mrzel, A., McCauley, J., O'Flaherty, S., McGuinness, C., Compagnini, G., Mihailovic, D., Blau, W.J., Coleman, J.N., 2005. J. Phys. Chem. B 109 (15), 7124–7133.
Ploscaru, M.I., Kokalj, S.J., Uplaznik, M., Vengust, D., Turk, D., Mrzel, A., Mihailovic, D., 2007. Nano Lett. 7 (6), 1445–1448.
Polsky, R., Gill, R., Kaganovsky, L., Willner, I., 2006. Anal. Chem. 78 (7), 2268–2271.
Popov, I., Gemming, S., Okano, S., Ranjan, N., Seifert, G., 2008a. Nano Lett. 8 (12), 4093–4097.
Popov, I., Pecchia, A., Okano, S., Ranjan, N., Di Carlo, A., Seifert, G., 2008b. Appl. Phys. Lett. 93 (8), 083115 (1–3).
Radi, A.E., AceroSanchez, J.L., Baldrich, E., O'Sullivan, C.K., 2006. J. Am. Chem. Soc. 128 (1), 117–124.
Sadik, O.A., Aluoch, A.O., Zhou, A., 2009. Biosens. Bioelectron. 24 (9), 2749–2765.
Sánchez, J.L.A., Baldrich, E., Radi, A.E.G, Dondapati, S., Sánchez, P.L., Katakis, I., O'Sullivan, C.K., 2006. Electroanalysis 18 (19–20), 1957–1962.
Steel, A.B., Herne, T.M., Tarlov, M.J., 1999. Bioconjug. Chem. 10 (3), 419–423.
Stojanovic, M.N., Landry, D.W., 2002. J. Am. Chem. Soc. 124 (33), 9678–9679.
Strle, J., Vengust, D., Mihailovic, D., 2009. Nano Lett. 9 (3), 1091–1095.
Sun, N., McMullan, M., Papakonstantinou, P., Gao, H., Zhang, X., Mihailovic, D., Li, M., 2008. Anal. Chem. 80 (10), 3593–3597.
Uplaznik, M., Bercic, B., Strle, J., Ploscaru, M.I., Dvorsek, D., Kusar, P., Devetak, M., Vengust, D., Podobnik, B., Mihailovic, D.D., 2006. Nanotechnology (17), 5142.
Vrbanic, D., Remskar, M., Jesih, A., Mrzel, A., Umek, P., Ponikvar, M., Jancar, B., Meden, A., Novosel, B., Pejovnik, S., Venturini, P., Coleman, J.C., Mihailovic, A., 2004. Nanotechnology 15, 635–638.
Wang, X., Lieberman, M., 2003. Langmuir 19 (18), 7346–7353.
Willner, I., Zayats, M., 2007. Angew. Chem. Int. Ed. 46 (34), 6408–6418.
Xiao, Y., Lubin, A.A., Heeger, A.J., Plaxco, K.W., 2005a. Angew. Chem. 44 (34), 5456–5459.
Xiao, Y., Piorek, B.D., Plaxco, K.W., Heeger, A.J., 2005b. J. Am. Chem. Soc. 127 (51), 17990–17991.
Yu, H.Z., Luo, C.Y., Sankar, C.G., Sen, D., 2003. Anal. Chem. 75 (15), 3902–3907.
Zhao, Q., Li, X.-F., Le, X.C., 2008. Anal. Chem. 80 (10), 3915–3920.
Zhou, L., Ou, L.-J., Chu, X., Shen, G.-L., Yu, R.-Q., 2007. Anal. Chem. 79 (19), 7492–7500.

Please cite this article in press as: McMullan, M., et al., Biosens. Bioelectron. (2010), doi:10.1016/j.bios.2010.01.030